2024 IEEE International Conference on Robotics and Automation (ICRA 2024)
May 13-17, 2024. Yokohama, Japan

Torque Transmission in Double-Tendon Sheath Driven Actuators for Application in Exoskeletons

Daniel Pérez-Suay*, Yu Li*, Hamid Sadeghian, Abdeldjallil Naceri and Sami Haddadin

***Abstract*— Bowden cables serve as essential components in various mechanical systems, facilitating power transmission from remote actuators to specific destinations. The pretension of Bowden cables profoundly influences system performance, notably in terms of friction. This study investigates the effects of cable pretension and shape on friction and torque efficiency. A custom self-designed testbed, comprising integrated actuator units, pulleys, and a novel pretension mechanism connected by Bowden cables, is utilized to conduct experimental tests under varying parameters. This work adopts an integrated approach of experimentation, modeling, and validation, offering preliminary insights into the torque transmission characteristics of tendon driven actuator systems. Additionally, the precise model exhibits excellent conformity across a broad range of shapes and provides initial insights into hysteresis modeling attributable to cable material properties.**

I. INTRODUCTION

As the global elderly population continues to expand, there is a growing need for home healthcare services, primarily due to the limited availability of healthcare workers (HCWs). One promising solution to address this shortage and provide greater flexibility to HCWs in terms of patient management and scheduling is the utilization of home healthcare robots, exemplified by GARMI [1]. Force-sensitive exoskeletons, designed for robotic teleoperation with haptic feedback, enable HCWs to employ GARMI as a surrogate or "mechanical avatar" [2] in remote healthcare scenarios.

At the Geriatronics Research Center, we are developing a lightweight exoskeleton for rehabilitation and assistive technology (as shown in Fig 1), exploring its use in controlling remote robots [3]. The performance of this exoskeleton mainly depends on its cable-based drive unit, with cable friction playing a crucial role in system control optimization. This study reveals the design of the new drive unit and explores the importance of different parameters on its power transmission.

One critical factor that significantly influences the overall performance of Bowden cables is the tension applied to the cable during operation [4]. The tension in Bowden cables is responsible for maintaining the desired level of force transfer, accuracy, and efficiency in motion transmission [5]. However, it is well recognized that the tension of the Bowden cables also has a profound impact on the friction characteristics within the cable system [6].

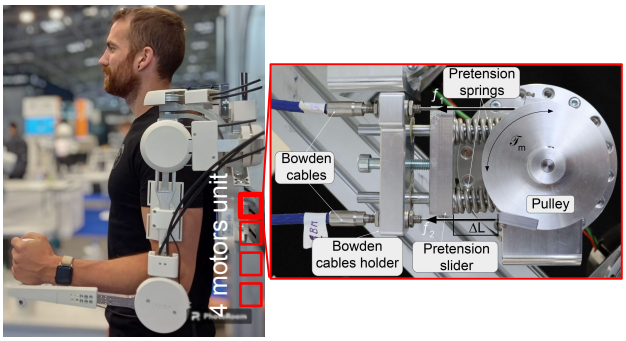

Fig. 1: The lightweight Exoskeleton with its integrated drive unit located in the backpack. The power is transmitted through Bowden cables. The design of the pretension mechanism is also illustrated.

The effect of friction plays a crucial role in Bowden cable systems as it directly affects the smoothness of motion, energy efficiency, and accuracy of the transmitted force [7]. Friction arises from the interaction between the inner core wire and the outer sheath, leading to resistive forces that impede the desired motion. Understanding the relationship between cable tension and friction is of paramount importance in optimizing the performance and reliability of Bowden cable systems [8].

Although several studies have investigated the frictional behavior of Bowden cables [9], [10], [11], limited research has been conducted specifically on the influence of cable tension. The existing literature primarily focuses on the design aspects of the cable and the selection of appropriate materials to reduce friction. However, a comprehensive understanding of how cable tension affects friction is crucial for designing efficient Bowden cable systems.

Considerable research has focused on modeling frictional forces to understand torque and force transmission. Coulomb friction models, including Stribeck-Coulomb variants, effectively quantify friction [12]. However, they fail to explain hysteresis phenomena [13]. To address hysteresis in tendon-driven mechanisms, studies have employed differential equation-based models [14] and [15], simulating infinitesimal surface contacts like the Dahl model [16]. Adaptations such as the LuGre model enhance dynamic properties and introduce friction coefficient variations [17], [18]. Ad-

All authors are with the Munich School of robotics and Machine Intelligence, Technical University of Munich, 80992 München, Germany. Corresponding Author: daniel.perez-suay@tum.de

*Both authors have equal contributions.

We gratefully acknowledge the funding of the Light- house Initiative Geriatronics by StMWi Bayern (Project X, grant no. IUK-1807-0007// IUK582/001) and LongLeif GaPa gGmbH (Project Y). The authors acknowledge the financial support by the Federal Ministry of Education and Research of Germany (BMBF) in the program of "Souver an. Digital. Vernetzt." Joint project 6G-life, project identification number 16KISK002. S. Haddadin has a potential conflict of interest as a share- holder of Franka Emika GmbH

ditionally, the Bouc-Wen model, widely used in modeling frictional hysteresis, offers modification capabilities [19] and finds applications in piezoelectric actuator designs [20].

Wu et al. [5] presented a model for double-tendon sheath driven actuators, considering cable elongation and material elasticity. However, it overlooks the tension distribution [21], [22] and varying velocity along the tendon path [23]. A lumped parameter model, addressing these issues, was developed for tendon sheath actuation [23], [24], [17], [18], capturing cable dynamics, force transmission, and displacement effects more comprehensively. However, these adaptations fail to account for pretension and its distribution, a key element in torque transmission efficiency. Additionally, tension sensors, as described in [5], [23], negatively affect material integrity.

This paper focuses on proposing a model for torque transmission in double-tendon sheath driven actuators, particularly emphasizing friction and transmission features. To improve the understanding of these systems by identifying and modeling the key features and dynamics, experimental validation is conducted on a testbed to establish the torque transmission relationship, integrating shape and force/torque sensing to corroborate our findings.

In the following sections, the system design, transmission modeling, and experimental results are presented. A discussion of the implications and practical considerations for modeling Bowden cable systems are given in the following.

II. System Description and Modeling

A. System Design

A novel testbed has been developed to conduct more detailed studies of tendon driven actuation systems. The setup consists of two motors coupled with two pulleys named as A and B. Two Bowden cables are mechanically fixed to the pulleys. The pretension is measured by load cells located on both sides through a pretension mechanism as illustrated in Fig. 2a.

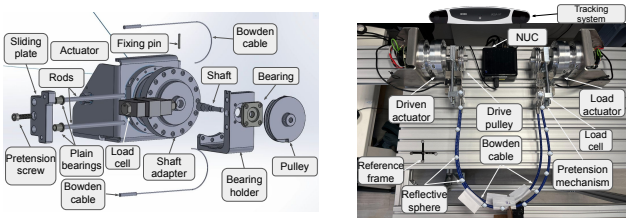

(a) (b)

Fig. 2: The exploded view of the pretension unit can be seen in (a). The mechanism is coupled to the actuator unit and the system allows us to regulate the pretension of the cables with high precision. On (b), Our proposed Bowden Cable testbed is shown.

The actuation unit on both sides consists of a harmonic drive motor, an encoder, and a torque sensor. The maximum torque of the motor is limited to 87Nm. By directing the τ_{in} to motor A, and subsequently inducing cable oscillations characterized by sinusoidal or damping profiles, the resultant τ_{out} torque of motor B is registered. A mechanical adapter was designed to hold the shaft, the load cell (Bosche and model S20S-C3-0100 with a nominal load of 100kg), and a plate that holds the Bowden cables. Tightening the screw at the plate against the load cell the pretension is produced at the Bowden cables and the value of pretension can be obtained from the load cell.

Additionally, a visual tracking system from NDI has been included to our setup, a crucial component for accurately monitoring the position of a cable's shape. Markers are strategically fixed to the cable, enabling real-time coordinate recording. Utilizing spline interpolation, we employ this recorded data to estimate and visualize the cable's shape. The visual system returns a set of spatial positions of markers. To have a clear interpretation, a reference frame was fixed on the testbed, such that the markers possibly aligned on a plane, since only 2D configuration is considered for the testbed scenario.

The testbed described above is driven by an Asrock NUC which operates a Linux operating system with a real-time kernel at a frequency of 1 kHz. A graphic description of the setup can be found in Fig. 2b.

The schematic of the testbed is shown in Fig. 3a. The testbed must have at least one of the two motors fixed to it to guarantee that the pretension of the cable can be measured by the load cell in straight shape. This will be further discussed in Section II-B. The symmetric structure of the testbed allows to conduct versatile studies. However, in this paper, we focus on the friction modeling of the double Bowden cable system. Therefore, motor A will be used as the active actuator to drive the system. Whereas, motor B will not only be used as a sensing unit (e.g., torque sensor and encoder) but also to apply dynamic loads to the system during the experiments.

B. Pretension Mechanism

The pretension of the Bowden cable is not only crucial for the transmission and performance of the system but also plays a significant role in the system's friction behavior [5], [23], [6], [25]. We developed a novel pretension mechanism to conduct a more detailed study on the effect of pretension on system performance and friction.

The free-body diagram of the whole testbed is shown in Fig. 3c. The prismatic joint of motor B allows free motion in x-direction. In steady-state conditions the force at joint A in x-direction is equal to:

$$T_{A,x} = 0. \tag{1}$$

The equilibrium equation for the free-body diagram in Fig. 3b is as follows:

$$\begin{aligned} x &: T_{A,x} + T_{O1,x} + T_{O2,x} - T_{L,x} = 0, \\ M_z &: (-T_{O1,x} + T_{O2,x})r = 0, \end{aligned} \tag{2}$$

where $T_{i,x}$ denotes the reaction forces in x-direction for $i \in \{A, B, O1, O2, L\}$. Combining the equations (1) and (2), the pretension $T_{O,x}$ in both cables is equal to the half of the force

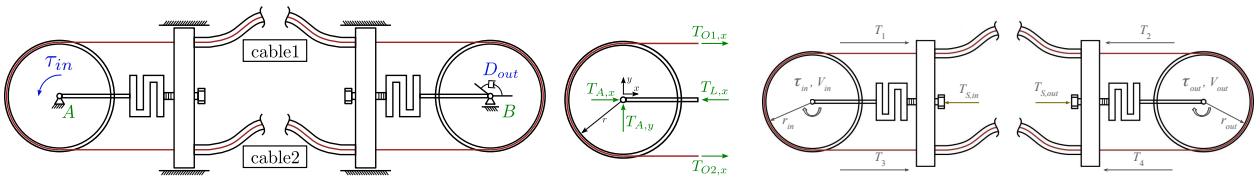

(a) (b) (c)

Fig. 3: Free-body diagrams. (a) Schematic of the double Bowden cable testbed. Where T_{in} denotes the input torque and D_{out} is the damping constant on the output side B. (b) The free-body diagram of the active motor A side in steady-state conditions. The pretension of the cable is equal to half of the measured by the load-cell. (c) The free-body diagram of the whole testbed, the notation used in this image is employed in section III.

measured by the load-cell $T_{L,x}$:

$$T_{O1,x} = T_{O2,x} = T_{O,x},$$
$$T_{O,x} = \frac{T_{L,x}}{2}. \tag{3}$$

It needs to be mentioned that two individual Bowden cables are used (see Fig. 3), and they are fixed to the pulleys/motors A, B. Therefore, $T_{O1,x}$ and $T_{O2,x}$ are mechanically coupled, and there is no friction relation between those two forces.

III. Torque Transmission Modeling

This section examines the torque transmission modeling specific to double-tendon sheath actuators, with a focus on the challenges arising from transmission efficiency impacted by inherent contact friction under pretension. In contrast to single-tendon systems where input force significantly affects system friction (as elaborated in [26] for subsequent cases), the influence of input torque on friction in double-tendon systems is relatively minor. However, in both systems pretension and curvature exert significant influence on friction in double-tendon systems, as detailed in section section IV-A. Consequently, it is prudent to approach double-tendon sheath driven mechanisms and single-tendon driven mechanisms differently.

Pretension was initially applied and is represented by tendon elongation. Both pretension and elongation remain constant during operation, as outlined in section III-B.

A. Cable Shape Modeling

The marker coordinates (x, y) along the sheath captured will be sorted from proximal to distal end (motor A to B). The sorted coordinates (x, y) will be interpolated via cubic spline w.r.t. a common coordinate t, which is the sequence of the markers, with "*spline*" in MATLAB. Then, the interpolated coordinates are processed w.r.t. the unified smooth common coordinate t_{smooth} up to N samples with "*ppval*" in MATLAB, considering $N = 500$.

This returned N smoothed waypoint $(x, y)_{smooth}$ of the tendon path provides the computation of the total bending angle θ along the arc length coordinate s, since

$$ds = \sqrt{x'^2_{smooth} + y'^2_{smooth}}\, dt_{smooth}. \tag{4}$$

Along with the curvature computation:

$$\kappa = \frac{|x'_{interp} y''_{smooth} - y'_{smooth} x''_{smooth}|}{(x'^2_{smooth} + y'^2_{smooth})^{3/2}}, \tag{5}$$

where $'$ and $''$ denote the first and second derivative w.r.t. the path variable t_{smooth}. With the total integration of the curvature κ, the total wrapped angle of the tendon path results as $\theta = \int_0^L \kappa ds$ or as computed in discrete case $\theta = \sum_{k=1}^{N-1} \kappa_k s_k$. For illustration is presented in Fig. 4.

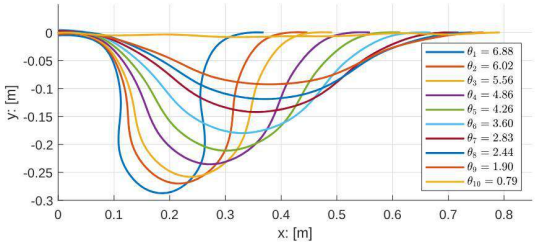

Fig. 4: Different cable shape in the planar case. Denote d_i with two ends distance, assuming they are axially aligned. $d_1 = 34.5, d_2 = 42.5, d_3 = 47, d_4 = 54, d_5 = 59, d_6 = 64.5, d_7 = 69.5, d_8 = 72, d_9 = 74, d_{10} = 77$ in cm. Corresponds with different total bending (wrapped) angles.

B. Transmission Modeling

In this section, we redirect our focus from the bending angle to the pivotal significance of curvature as a fundamental system characteristic [27]. Consequently, the modeling of transmission has been predicted based on the curvature, which is linked to the shape of the cable. From infinitesimal cable segment force analysis, we have,

$$T_{out} = T_{in} e^{\lambda \mu \int_0^L \kappa(s) ds} = T_{in} e^{\lambda \mu \theta}, \tag{6}$$

and

$$\Delta L = \int_0^L \left(\frac{T_{in} e^{-\mu \int_0^s \kappa(\sigma) d\sigma} - T_{O,x}(s)}{EA}\right) ds, \tag{7}$$

where the $T_{in/out}$ denotes the input/output tension force of the tendon, and ΔL represents cable elongation. $T_{O,x}(s)$ denotes the pretension force, which is not uniformly distributed along the arc length s [21], [23], [28]. The parameters E and A denote Young´s modulus and cross-section area of the tendon respectively, and λ denotes the motion direction equal to 1 or -1. Parameter μ is the frictional coefficient. The total wrapped angle notation θ can not be simplified from curvature integration in (7) since no constant curvature assumption has been used.

To consider the force transmission on the double-tendon sheath driven actuators, from (6), the force on each cable is

given as

$$T_2 = T_1 e^{-\mu\theta} = \alpha T_1, \tag{8}$$

$$T_4 = T_3 e^{\mu\theta} = \beta T_3, \tag{9}$$

Fig. 3c is referred to for notation conventions.

The elongation in operation is considered as (7), regarding the applied tension from the input motor producing active torque τ_{in} to pull the upper cable and given as,

$$\begin{aligned}\Delta L_u &= \frac{\int_0^L (T_1 e^{-\mu \int_0^s \kappa(\sigma)d\sigma} - T_{O,x}(s))ds}{EA} \\ &= \frac{\int_0^L (T_1 e^{-\mu \int_0^s \kappa(\sigma)d\sigma})ds - \int_0^L (T_s e^{-\mu \int_0^s \kappa(\sigma)d\sigma})ds}{EA} \\ &= \frac{\Psi_\alpha T_1 - C_{T_O}}{EA},\end{aligned} \tag{10}$$

with

$$\Psi_\alpha = \int_0^L (e^{-\mu \int_0^s \kappa(\sigma)d\sigma})ds, \tag{11}$$

$$C_{T_O} = \int_0^L (T_s e^{-\mu \int_0^s \kappa(\sigma)d\sigma})ds, \tag{12}$$

where $T_s = \frac{T_{s,in}+T_{s,out}}{4}$ is the average load cell value and is treated as the known pretension value at boundary of the tendon, therefore, the integrated term in C_{T_O} follows the same way of (6). The pretension related-term C_{T_O} has to be isolated under the assumption, that the total elongation of each cable inducted from the pretension kept the same during operation,

Similarly, the elongation of the lower cable reduces tension force since the upper cable has been pulled, the elongation is adjusted with opposite motion direction,

$$\begin{aligned}\Delta L_l &= \frac{\int_0^L (T_3 e^{\mu \int_0^s \kappa(\sigma)d\sigma} - T_{O,x}(s))ds}{EA} \\ &= \frac{\Psi_\beta T_3 - C_{T_O}}{EA},\end{aligned} \tag{13}$$

with

$$\Psi_\beta = \int_0^L (e^{\mu \int_0^s \kappa(\sigma)d\sigma})ds. \tag{14}$$

Note that, the pretension-related term C_{T_O} is the same since the cable pair shapes are considered to be the same.

Under the assumptions, 1) the mass/inertia of pulleys and tendon are negligible, 2) the tendon kept taught in operation under pretension effect, the following equations are given,

$$\tau_{in} = r_{in}(T_1 - T_3), \tag{15}$$

$$\tau_{out} = r_{out}(T_2 - T_4), \tag{16}$$

$$\Delta L_u + \Delta L_l = 0. \tag{17}$$

Incorporating (17) and integrating with (10) and (13) for two cables, in conjunction with the torque equations (15) and (16) of force, the resultant torque transmission equation is derived as follows,

$$\tau_{out} = K_{in}\tau_{in} + K_{T_O}C_{T_O}, \tag{18}$$

where, $K_{in} = \frac{r_{out}(\Psi_\beta\alpha + \Psi_\alpha\beta)}{r_{in}(\Psi_\alpha + \Psi_\beta)}$ and $K_{T_O} = \frac{2r_{out}(\alpha-\beta)}{\Psi_\alpha + \Psi_\beta}$.

C. Velocity Dependency

The hysteresis start/end states can be conducted by determining the velocity. μ can be adopted to Stribeck-Coulomb function as

$$\mu = \mu_d + (\mu_s - \mu_d)e^{-|\frac{v}{\nu_s}|^2} \tag{19}$$

Due to factors such as limited operational environments or constrained output side designs, the input velocity is often utilized as the hysteresis signal. However, this assumes cable rigidity, which may not always be applicable due to cable compliance [24]. It is introduced with a smooth dead-zone function for velocity, which operates under the assumption that velocities within a narrow range suggest minimal induced motion, as follows,

$$v_{hys} = 0.5\tanh\left((s_v\left(v^2 - v_{thres}^2\right)\right) + 0.5, \tag{20}$$

where v_{hys}, v, v_{thres} denotes the hysteresis state velocity, input velocity, and the dead-zone threshold velocity of the function, respectively. Parameter s_v is a scalar and tunes the slope of the $\tanh$ function. The output torque prediction is adopted to have memory function,

$$\begin{aligned}\tau_{out} &= \boldsymbol{v}^T\boldsymbol{\tau}, \\ \boldsymbol{v} &= [v_{hys} \quad v_{hys}\,\mathrm{sign}(v) \quad 1 - v_{hys}]^T, \\ \boldsymbol{\tau} &= \left[K_{in}\tau_{in} \quad K_{T_O}C_{T_O} \quad \tau_{out}(t^-)\right]^T,\end{aligned} \tag{21}$$

where $\tau_{out}(t^-)$ denotes the last memorized output torque value.

IV. Result And Discussion

The experiments for data acquisition have been conducted for feature observation and model fitting. The desired input torque trajectories are applied to both, the input motor system and the model. On the output side, a control command is given as $\tau = -K_p(q - q_{init}) - K_d\dot{q}$ is applied, to resemble a spring-damper load with positive constants K_p and K_d w.r.t. the initial motor position q_{init}.

A. Preliminary Results

The torque transmission equation (18), incorporates a slope denoted as K_{in} and an offset termed $K_{TO}C_{TO}$. The results reveal that K_{in} is close to 1 during the pure sliding phase, where the varying slope phase overpass the pre-sliding phase, as illustrated in Fig. 5a(1), Fig. 5b(1) and Fig. 6b(1).

Fig. 5a shows the friction effect strongly related to the pretension magnitude. This fact can be seen either in input/output torque relation for the offset in Fig. 5a(1) or the friction torque magnitude computed by $\tau_{fric} = \tau_{in} - \tau_{out}$ as represented in Fig. 5a(2), under same cable shape condition.

Simultaneously, it is noteworthy that the configuration of the cable affects the frictional impact under identical pretension conditions, as illustrated in Fig. 5b. Specifically, a greater degree of bending or curvature in the cable shape correlates with increased frictional effects. It is important to acknowledge a minor variation in pretension measurements, which may be attributed to pretension loss caused by the gap between the tendon diameter and the sheath inner diameter [29]. Moreover, it is observed that higher degrees of cable bending result in slightly greater tendon elongation losses.

Besides, to illustrate the hysteresis characteristic resulting from material compliance and friction as documented by Agrawal et al. [23], Fig. 6b(2) exhibits a comparable Stick-Slip effect, which is further addressed by Zheng et al. [30] and Drincic et al. [31]. However, the friction torque computed from the difference between input/output torque does not result in a classical Stick-Slip effect (see the zoomed view in Fig. 6b(2)). The phenomenon of the disorderly friction torque trajectory occurs predominantly after alterations in motion or changes in input torque direction. In such instances, the output side retains a memory of the last attainable output torque. The computed friction torque during this phase is determined by how the input torque varies. One can inspect the input/output torque dynamic phenomena from the time plot (Fig. 6a), where the input torque of a frequency combination (see Table I for τ_{in}) frequently varies under maximal stiction friction. According to Fig. 6a and Fig. 6b(1), the output torque is memorized at some low magnitude, for the case that the input torque is less than maximal stiction friction. Therefore, the model is proposed in an input/output torque modeling way instead of directly modeling the friction, which facilitates the identification.

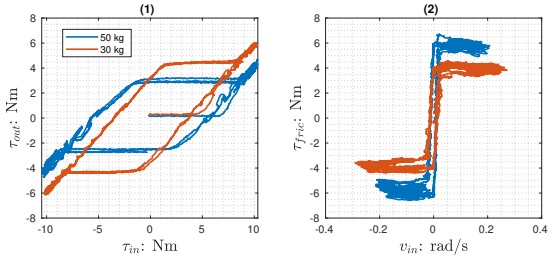

(a)

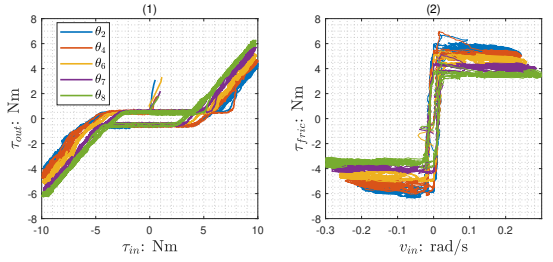

(b)

Fig. 5: (a) the input-output relation w.r.t. two significantly different load cell values (pretension) in (1), and frictional difference w.r.t. the input velocity in (2). This result was recorded under the shape θ_1. (b) depict the input-output relation w.r.t different shapes in (1) and frictional difference in (2). Their corresponding pretension is measured in [51.83, 52.07, 53.29, 53.91, 54.08] kg.

B. Model Fitting

To obtain and validate the proposed model w.r.t. concerned factors that may influence the torque transmission performance, the experiment is designed to collect data for different shapes, frequencies, and pretensions. It is worth noting that the pretension is read for each group respectively. The dataset is assembled according to the specifications outlined in Table I, covering up to 10 groups exhibiting diverse shapes, as illustrated in Fig. 4.

Load cell $T_{s,i}$	**Shape** θ_i	**Frequency** f
$T_{s,1}$	θ_1	$f = \frac{1}{5s}$
		$f = \frac{1}{7s}$
$T_{s,2}$	θ_2	$f = \frac{1}{10s}$
		f_{sup}
$T_{s,i}$	θ_i	...

TABLE I: Data set for model identification and validation for different shape and pretension conditions. $T_{s,i}$ is the corresponding pretension for different shape groups. f_{sup} is the notation for a torque trajectory with superposed frequencies $\tau_{in} = A\left(\sin(\cdot 2\pi\frac{t}{T_p}) + \frac{1}{3}\sin(3\cdot 2\pi\frac{t}{T_p}) + \frac{1}{5}\sin(5\cdot 2\pi\frac{t}{T_p})\right)$ with A for amplitude and T_p for period time, which is presented as an instance in Fig. 6a. $T_{s,i}$, θ_i, and ... present more collected data groups, that possess the considered features in various magnitude.

Additionally, an optional frequency experiment has been conducted for each group. It is expected that an arbitrary group data from the Table I can fit the model and determine the model parameters $\boldsymbol{p} = [\mu_d, \mu_s, \nu_s, v_{thres}, s]$. The model is implemented on MATLAB by optimizing the object function $\textbf{MSE} = \frac{1}{N}\sum_{i=1}^{N}(\tau_{out}(i) - \hat{\tau}_{out}(i))^2$ with multivariate-derivative-free approach "*fminsearch*". The determined parameter given in $\boldsymbol{p}$ = $[0.056, 0.062, 0.546, 0.884, 1283.334]$ is obtained based on the data from θ_6 under load cell reading $T_s = 54kg$. It shows that the static friction coefficient is slightly greater than the dynamic friction coefficient, which matches our premise. An experiment related to material friction coefficient in cable conduit systems was provided in [32] for literature insight.

C. Model Validation and Discussion

1) Different Shapes: The model accurately aligns with the magnitude at the specified low frequency, as shown in Fig. 7. This alignment corresponds with the detailed analysis of the torque transmission model under pretension, effectively addressing the static challenge. It is remarkable that at the hysteresis phase, where the output torque remains unchanged. Besides, it can be observed that the mean value of the prediction error is relatively small. However, the groups θ_7 and θ_8 have slightly larger bias around where the output torque remains unchanged, which is primarily attributed to the limited accuracy in predicting hysteresis (see Section IV-C.3 for more details).

2) Different Pretensions: The validation outcome for scenarios where the pretension varies substantially is displayed in Fig. 8 under the same cable shape. The proposed model performs very well in terms of magnitude for load cell value of 50 kg. However, in the 30 kg pretension, slight overestimation is observed, particularly in the highest torque range. This discrepancy is because of potential pretension loss due to experimental factors, such as reduced lubrication of the pretension guiding mechanism (see Fig. 2a), which

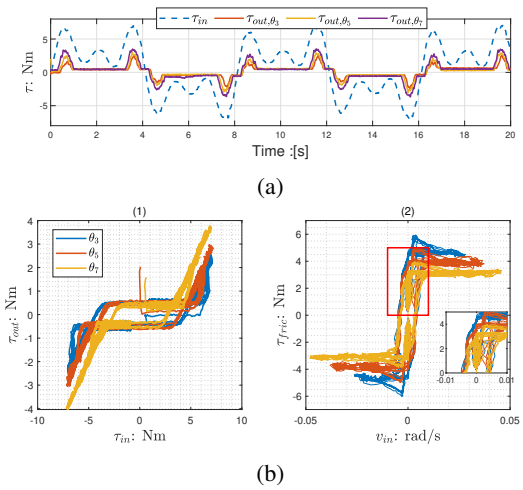

Fig. 6: (a) presents firstly, the torque transmission loss w.r.t. different cable shapes and, secondly, hysteresis phenomena where the input torque varies, the output torque remains unchanged. (b) presents the preliminary result of the torque transmission up to different shapes (refer to Fig. 4 for shape definition), adopted based on (a). (1) presents the input-output relation hysteresis loop. (2) presents the friction torque, with zoomed view on the pre-sliding phase w.r.t. the input velocity.

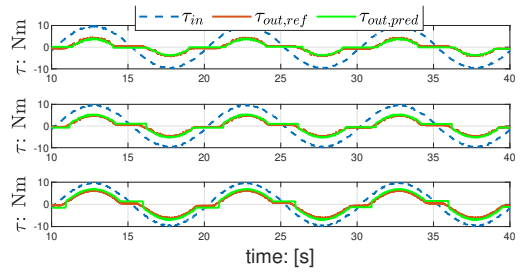

Fig. 7: Model validation w.r.t. different shapes, from top to bottom are with θ_2, θ_7, θ_8 with same frequency $f = 0.1Hz$. The MSE was computed in [0.254, 0.196, 0.271] N^2m^2.

might lead to unexpected displacement during the operation. Overall, for about 40% of the pretension difference, the model fits in an acceptable range.

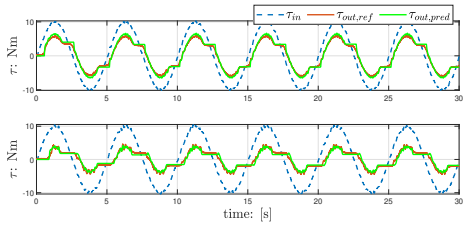

Fig. 8: Model validation results for the case of two different significant groups for pretension 30 kg (top), 50 kg (down). MSE is given in [0.245 0.294] N^2m^2. The frequency is set to be 5 Hz.

3) Hysteresis Fitness: The difficulty presented by hysteresis becomes more noticeable when accounting for the alternating directions of motion, as illustrated in Fig. 9. To validate the fitness on the hysteresis, the input torque trajectory with superposed frequencies has been applied, although in simple trajectory with sinusoidal form validations (Fig. 7 and Fig. 8) have shown its capability of correctly memorizing the output torque. The performance has correspondingly reduced according to the given MSE value, which can be concluded that the more dramatic dynamics inside cables, the hysteresis behavior became less easily to be captured by modified velocity observation.

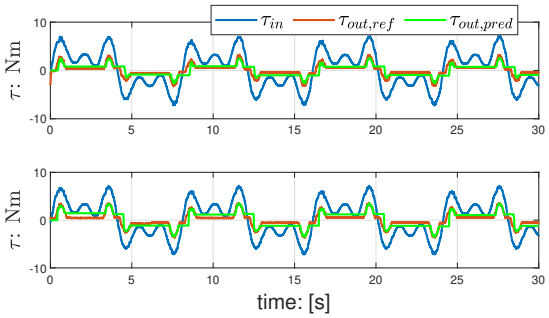

Fig. 9: The model validation results for the case with multiple frequency superposition with θ_5 (top), θ_7 (down). MSE is given in [1.006, 0.735] N^2m^2.

V. CONCLUSION

This study presents a compact design of a tendon-driven actuation system. To substantiate our assertion that pretension and cable shape are pivotal factors, a comparable experiment was conducted with summarizing the important features and knowledge. Based on that, we introduce a precise physical model incorporating velocity-dependent hysteresis modification. This model is validated to demonstrate the correlated torque transmission across various shape and pretension factors within a precise quality and shows its capability for fitting the hysteresis under different conditions. The results of the paper illustrate an experimental, modeling, and validation approach, offering more insights into the torque transmission characteristics of tendon-driven actuator systems. Additionally, the precise model demonstrates excellent conformity in terms of magnitude across diverse shapes within a broad range, providing an initial understanding of hysteresis modeling attributable to cable material properties.

REFERENCES

[1] M. Tröbinger, C. Jähne, Z. Qu, J. Elsner, A. Reindl, S. Getz, T. Goll, B. Loinger, T. Loibl, C. Kugler, C. Calafell, M. Sabaghian, T. Ende, D. Wahrmann, S. Parusel, S. Haddadin, and S. Haddadin, "Introducing garmi - a service robotics platform to support the elderly at home: Design philosophy, system overview and first results," *IEEE Robotics and Automation Letters*, vol. 6, no. 3, pp. 5857–5864, 2021.

[2] M. Tröbinger, A. Costinescu, H. Xing, J. Elsner, T. Hu, A. Naceri, L. Figueredo, E. Jensen, D. Burschka, and S. Haddadin, "A dual doctor-patient twin paradigm for transparent remote examination, diagnosis, and rehabilitation," in *2021 IEEE/RSJ International Conference on Intelligent Robots and Systems (IROS)*. IEEE, 2021, pp. 2933–2940.

[3] A. Toedtheide, X. Chen, H. Sadeghian, A. Naceri, and S. Haddadin, "A force-sensitive exoskeleton for teleoperation: An application in elderly care robotics," in *2023 IEEE International Conference on Robotics and Automation (ICRA)*. IEEE, 2023, pp. 12 624–12 630.

[4] U. Jeong and K.-J. Cho, "Feedforward friction compensation of bowden-cable transmission via loop routing," in *2015 IEEE/RSJ International Conference on Intelligent Robots and Systems (IROS)*, 2015, pp. 5948–5953.

[5] Q. Wu, X. Wang, L. Chen, and F. Du, "Transmission model and compensation control of double-tendon-sheath actuation system," *IEEE Transactions on Industrial Electronics*, vol. 62, no. 3, pp. 1599–1609, 2015.

[6] D. Chen, Y. Yun, and A. D. Deshpande, "Experimental characterization of bowden cable friction," in *2014 IEEE International Conference on Robotics and Automation (ICRA)*, 2014, pp. 5927–5933.

[7] H. Vallery, J. Veneman, E. van Asseldonk, R. Ekkelenkamp, M. Buss, and H. van Der Kooij, "Compliant actuation of rehabilitation robots," *IEEE Robotics Automation Magazine*, vol. 15, no. 3, pp. 60–69, 2008.

[8] A. Schiele, P. Letier, R. Linde, and F. van der Helm, "Bowden cable actuator for force-feedback exoskeletons," 11 2006, pp. 3599 – 3604.

[9] J. D. Martin and J. Savall, "Mechanisms for haptic torque feedback," *First Joint Eurohaptics Conference and Symposium on Haptic Interfaces for Virtual Environment and Teleoperator Systems. World Haptics Conference*, pp. 611–614, 2005. [Online]. Available: https://api.semanticscholar.org/CorpusID:206866597

[10] G. Smit and D. Plettenburg, "Efficiency of voluntary closing hand and hook prostheses," *Prosthetics and orthotics international*, vol. 34, pp. 411–27, 12 2010.

[11] A. Goiriena, I. Retolaza, A. Cenitagoya, F. Martinez, S. Riano, and J. Landaluze, "Analysis of bowden cable transmission performance for orthosis applications," 05 2009, pp. 1 – 6.

[12] H. Olsson, K. J. Åström, C. C. D. Wit, M. Gäfvert, and P. Lischinsky, "Friction models and friction compensation."

[13] M. Dezman, T. Asfour, A. Ude, and A. Gams, "Mechanical design and friction modelling of a cable-driven upper-limb exoskeleton," *Mechanism and Machine Theory*, vol. 171, p. 104746, 05 2022.

[14] T. N. Do, T. Tjahjowidodo, M. W. S. Lau, and S. J. Phee, "Dynamic friction-based force feedback for tendon- sheath mechanism in notes system," *International Journal of Computer and Electrical Engineering*, vol. 6, pp. 252–258, 2014.

[15] T. Do, T. Tjahjowidodo, M. Lau, and S. Phee, "A new approach of friction model for tendon-sheath actuated surgical systems: Nonlinear modelling and parameter identification," *Mechanism and Machine Theory*, vol. 85, pp. 14–24, 2015.

[16] G. Palli and C. Melchiorri, "Model and control of tendon-sheath transmission systems," *Proceedings of the 2006 IEEE International Conference on Robotics and Automation*, pp. 988–993, 2006.

[17] G. Palli, G. Borghesan, and C. Melchiorri, "Modeling, identification, and control of tendon-based actuation systems," *IEEE Transactions on Robotics*, vol. 28, no. 2, pp. 277–290, 2011.

[18] G. Palli and C. Melchiorri, "Friction compensation techniques for tendon-driven robotic hands," *Mechatronics*, vol. 24, pp. 108–117, 3 2014.

[19] Z. Zhang, G. Zhang, S. Wang, and C. Shi, "Hysteresis modeling and compensation for tendon-sheath mechanisms in robot-assisted endoscopic surgery based on the modified bouc-wen model with decoupled model parameters," *IEEE Transactions on Medical Robotics and Bionics*, vol. 5, pp. 218–229, 5 2023.

[20] Q. Zhang, Y. Dong, Y. Peng, J. Luo, S. Xie, and H. Pu, "Asymmetric bouc–wen hysteresis modeling and inverse compensation for piezoelectric actuator via a genetic algorithm–based particle swarm optimization identification algorithm," *Journal of Intelligent Material Systems and Structures*, vol. 30, pp. 1263–1275, 5 2019.

[21] Z. Sun, Z. Wang, and S. J. Phee, "Modeling and motion compensation of a bidirectional tendon-sheath actuated system for robotic endoscopic surgery," *Computer Methods and Programs in Biomedicine*, vol. 119, pp. 77–87, 4 2015.

[22] R. V. P. F. A. Ilia G. Polushin, *Quasi-Static Modeling of the da Vinci Instrument*. IEEE, 2014.

[23] V. Agrawal, W. J. Peine, and B. Yao, "Modeling of transmission characteristics across a cable-conduit system," *IEEE Transactions on Robotics*, vol. 26, pp. 914–924, 2010.

[24] V. Agrawal, B. Yao, and W. J. Peine, "Modeling of viscoelastic cable-conduit actuation for mri compatible systems," *Journal of Dynamic Systems, Measurement, and Control*, vol. 135, 2013.

[25] I. S. B. Fabrizio Sergi, Member, "Dynamic modeling and state estimation of cable-conduit actuation during interaction with non-passive environments," *IEEE/ASME Transactions on Mechatronics*, 2020.

[26] Z. Shao, Q. Wu, B. Chen, H. Wu, and Y. Zhang, "Modeling and inverse control of a compliant single-tendon-sheath artificial tendon actuator with bending angle compensation," *Mechatronics*, vol. 63, 11 2019, spring effectsheath diameter effect.

[27] Y. Tang, M. Pan, Y. Lin, and K. Liang, "Research on force and position control performance of the tendon sheath system with time-varying parameters and flexible robotic arms," *International Journal of Medical Robotics and Computer Assisted Surgery*, 8 2023.

[28] Z. Sun, Z. Wang, and S. J. Phee, "Elongation modeling and compensation for the flexible tendon - sheath system," *IEEE/ASME Transactions on Mechatronics*, vol. 19, pp. 1243–1250, 2014.

[29] Q. Wu, X. Wang, B. Chen, and H. Wu, "Modeling, online identification, and compensation control of single tendon sheath system with time-varying configuration," *Mechanical Systems and Signal Processing*, vol. 130, pp. 56–73, 9 2019.

[30] X. Zheng, T. Yang, Z. Chen, X. Wang, B. Liang, and Q. Liao, "Ale formulation for dynamic modeling and simulation of cable-driven mechanisms considering stick–slip frictions," *Mechanical Systems and Signal Processing*, vol. 168, p. 108633, 2022.

[31] B. Drincic, "Mechanical models of friction that exhibit hysteresis, stick-slip, and the stribeck effect," Ph.D. dissertation, University of Michigan, 2012.

[32] G. C. Weitz, "Coefficient of friction measurement between cable and conduit surfaces under varying normal loads," *IEEE transactions on power apparatus and systems*, no. 1, pp. 16–21, 1985.